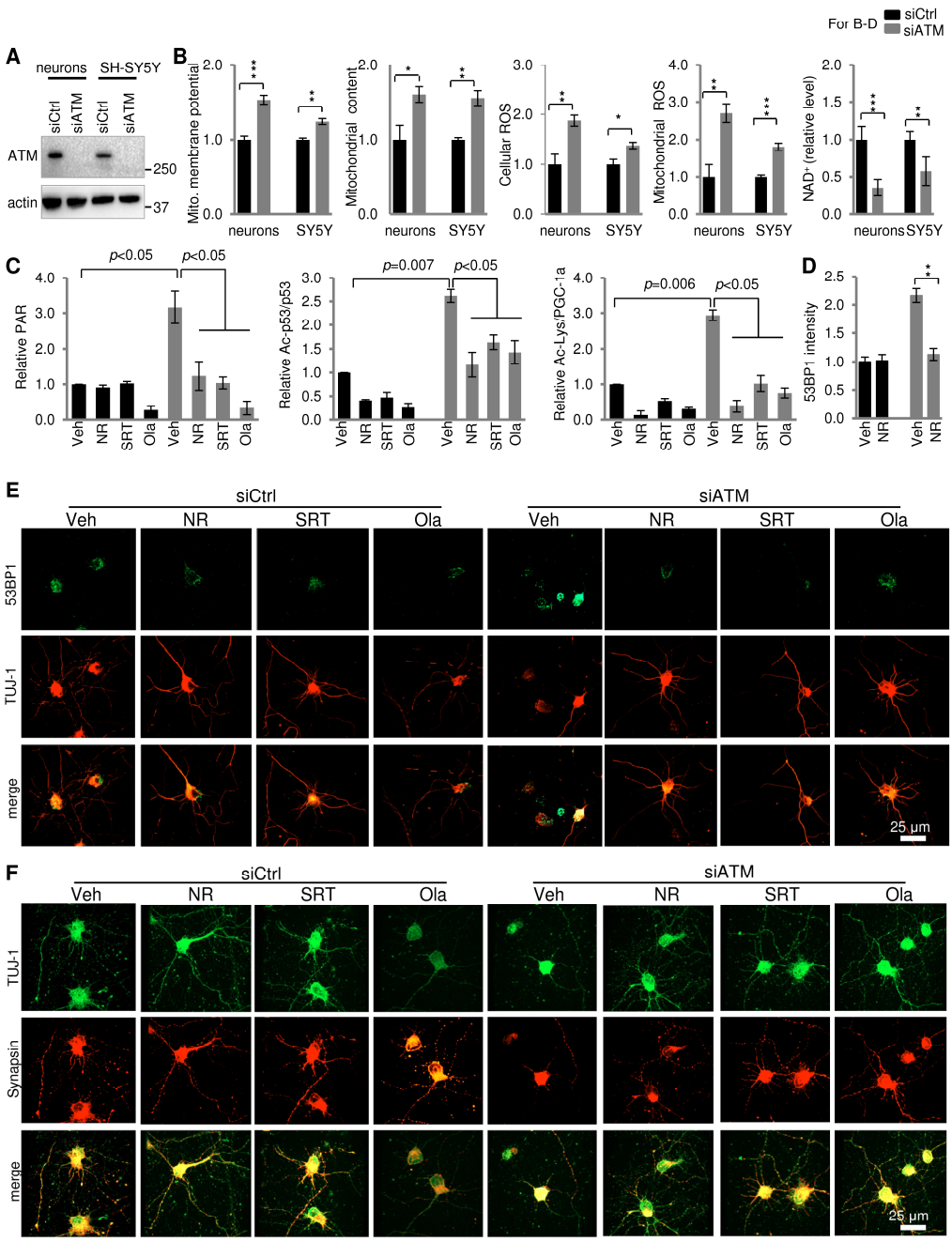

Sup Fig. 1.

Figure S1. Mitochondrial dysfunction in ATM-deficient neurons resulting from NAD$^+$/SIRT1 reduction (Related to Figure 1).

(A) Immunoblots showing knockdown efficiency of ATM by ATM siRNA on primary rat neurons and human neuroblastoma SH-SY5Y cells.

(B) Relative levels of mitochondrial membrane potential, mitochondrial content, cellular ROS, mitochondrial ROS, and cellular NAD^+ levels in WT and ATM-KD neurons or SH-SY5Y cells. Data are mean ± S.D. (n = 6-10 cultures/group). *$p < 0.05$, ** $p < 0.01$, or *** $p < 0.001$.

(C) Quantification of designated antigen levels. Data were from 2-3 repeats with a representative set shown in Fig. 1D.

(D) Quantification of 53BP1 intensity. Neurons of different groups were stained with 53BP1, TUJ-1 and images were taken using a confocal microscopy (Eclipse TE-2000e, Nikon). Fluorescent intensity of at least 30 neurons per group was measured. A representative set of images is shown in Fig. 1G.

(E) Representative confocal microscopy images of control and ATM-KD neurons after different treatments. Neurons were stained for the neuronal marker TUJ-1, and the DNA double-strand break marker 53BP1.

(F) Representative confocal microscopy images of WT and ATM-KD neurons after different treatments. Neurons were stained for a neuronal marker, TUJ-1, and the synapse marker, Synapsin. Rat cortical neurons at 3 days *in vitro* (DIV) were treated with either scrambled siRNA (siCtrl) or ATM siRNA (siATM) for three days. A 48 hour treatment of designated compounds was initiated at 5 DIV, followed by detection of multiple endpoints on 7 DIV. ATM was knocked down in SH-SY5Y cells using siRNA strategy. Veh, vehicle; NR, nicotinamide riboside, 500 μM; SRT1720/SRT, 2 μM; Ola, Olaparib, 500 nM.

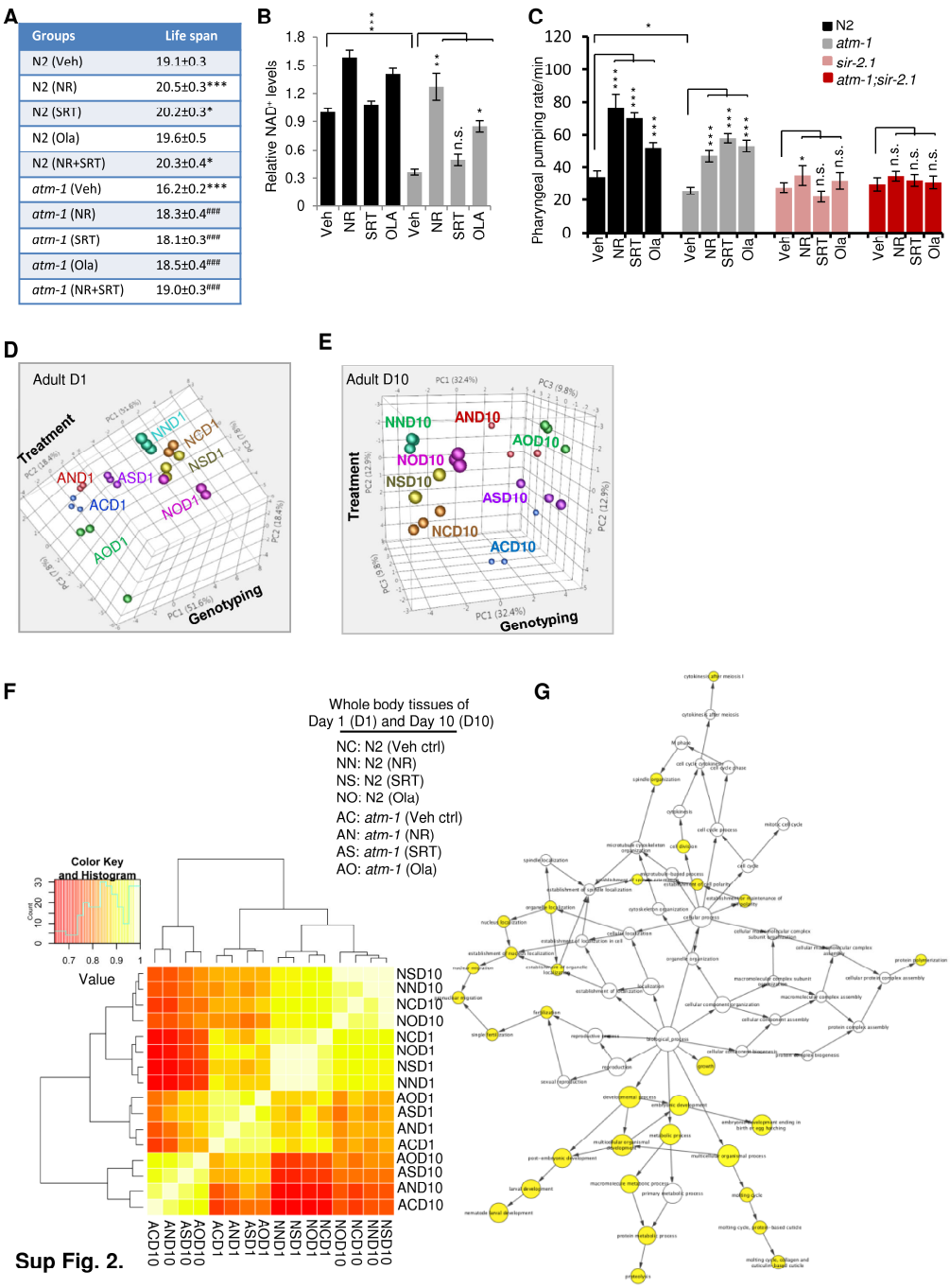

Sup Fig. 2.

Figure S2. Effects of NAD$^+$/SIR-2.1 pathway augmentation on the healthspan, transcriptional profile, and proteomics of N2 and *atm-1* mutant nematodes (Related to Figures 2 and 3)

(A) A summary of lifespans of N2 and *atm-1* worms (mean ± S.D.). Log-rank calculations were used to determine statistical significance. **p* < 0.05, ** *p* < 0.01, or *** *p* < 0.001 compared with N2 (veh); ### *p* < 0.001 compared with *atm-1* (veh). For curves, see Fig. 2.

(B) Relative NAD^+ levels in D7 adult worms. **p* < 0.05, ** *p* < 0.01, *** *p* < 0.001, and n.s., not significant.

(C) Pharyngeal pumping rate in adult D8 worms of the indicated strains with different treatments (mean ± S.E.M, n = 10-20 worms/group). **p* < 0.05, *** *p* < 0.001, and n.s., not significant.

(D-E) Principle component analysis of average gene expression Z scores of adult D1 or D10 worms. (F) Heat map analysis of proteomics results from all the 16 groups with acronym definitions on the right.

(G) Proteome-wide analysis of NR-treated D10 atm-1 reveals multiple health benefits after augmentation of the NAD+/SIR-2.1 pathway. Protein expression was significantly changed upon NR supplementation in old *atm-1* worms at D10 and thus were analyzed for enriched biological processes using Cytoscape in conjunction with the BiNGO plug-in. The yellow denotes significantly changed pathways. The size of the circles corresponds to the number of proteins changed.

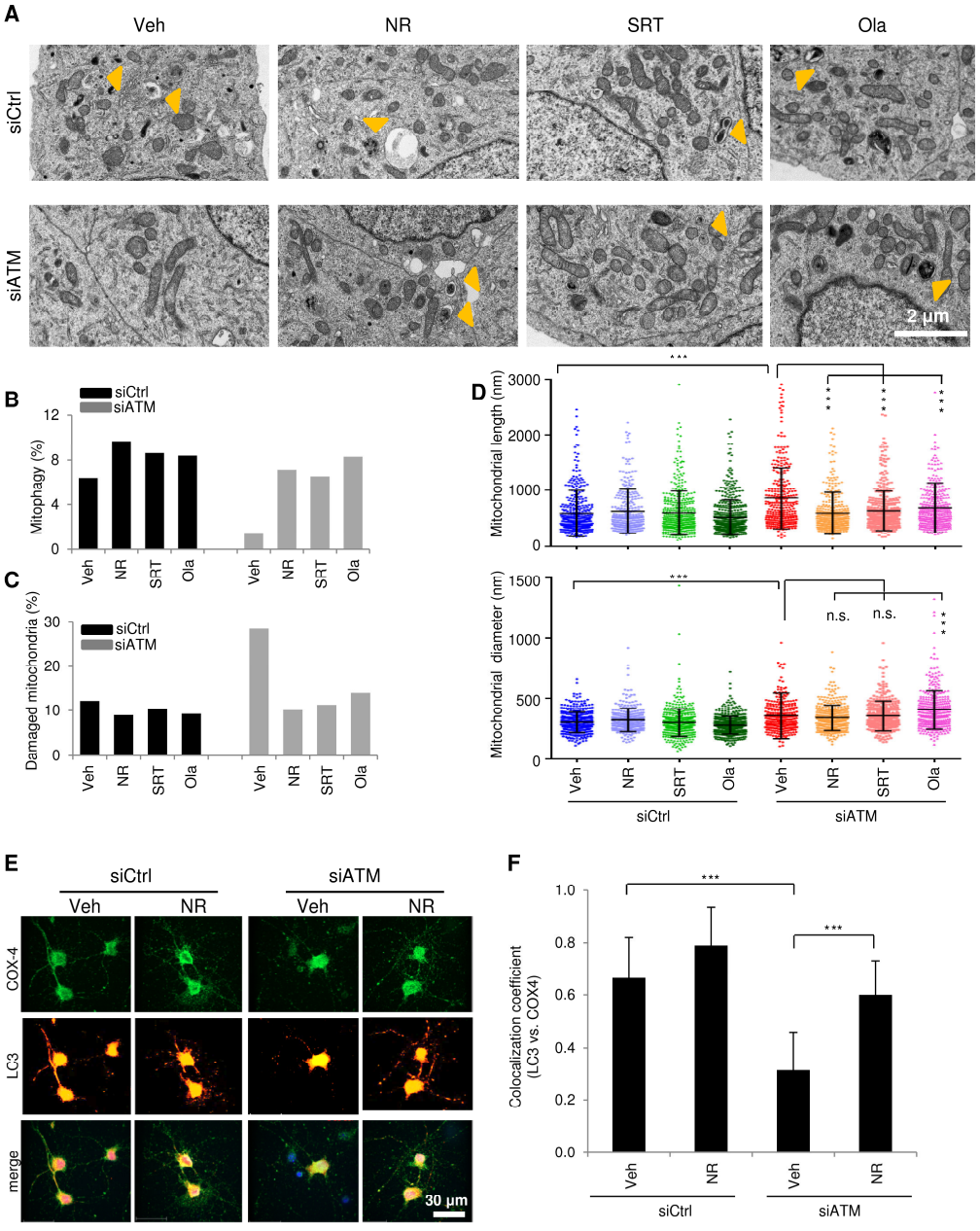

Sup Fig. 3.

Figure S3. Effects of NAD$^+$/SIRT1 pathway on mitochondrial homeostasis and mitophagy (Related to Figure 4).

(A) Representative electron microscopy (EM) pictures showing mitochondrial morphology of WT and ATM-KD SH-SY5Ycells after treatment with vehicle or 500 μM NR. A total of 14

pictures were randomly taken for each group. Mitochondria likely undergoing mitophagy (yellow arrow) were marked.

(B-C) Quantification of percentage of mitochondria undergoing mitophagy (B) and damaged mitochondria (C). These figures were identified in EM images from WT and ATM-KD SH-SY5Y cells with different treatments. A total of 306-514 mitochondria were analyzed.

(D) Quantification of mitochondrial length and diameter using EM images from WT and ATM-KD SH-SY5Y cells with different treatments. Mitochondrial diameter: WT veh, n =393; WT NR, n=306; WT SRT, n = 453; WT Ola, n = 514; ATM-KD veh, n = 319; ATM-KD NR, n = 375; ATM-KD SRT, n = 408; ATM-KD Ola, n = 363; Data shown are mean ± S.D.

(E-F) Rat primary cortical neurons at 3 DIV were treated with either scrambled siRNA (siCtrl) or ATM siRNA (siATM) for three days. On 5 DIV, cells were treated with NR (500 μM) for 48 h. Neurons were harvested on 7 DIV, and stained for the autophagy marker LC3 and a mitochondrial marker COX-4 before confocal imaging. The colocalization between LC3 and COX-4 was quantified using the Pearson's correlation coefficient (mean ± S.D.). Of note, images shown in figure (E) were intentionally overexposed to visualize neurites.

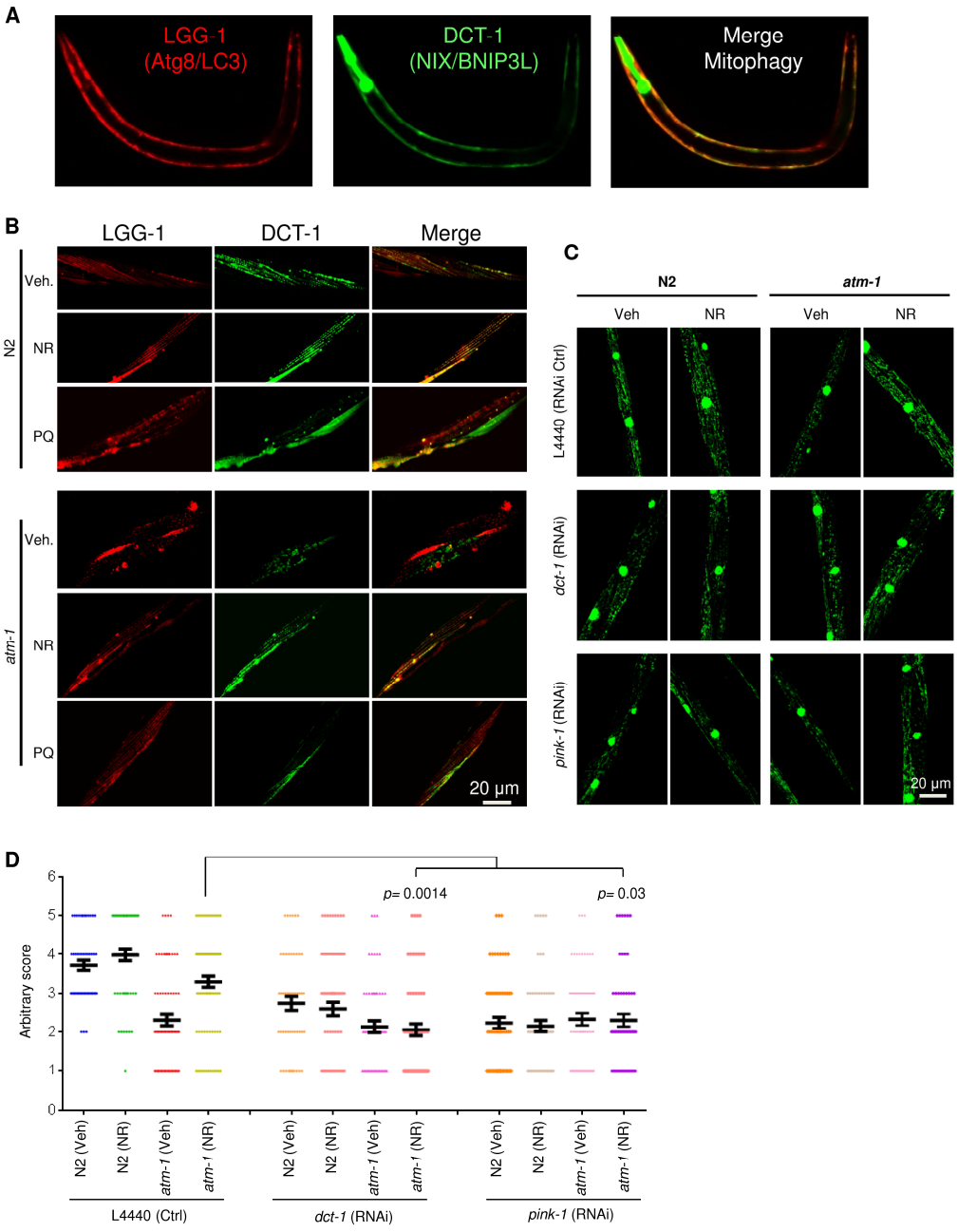

Sup Fig. 4.

Figure S4. Augmentation of NAD$^+$ levels restores mitophagy and improves mitochondrial network in *atm-1* worms (Related to Figure 4).

(A) A mitophagy-screening strain N2;*Ex(pmyo-3::dsred::lgg-1;pdct-1::dct-1::gfp)* was used for mitophagy detection. This transgenic strain expresses two fluorescent proteins, the DCT-

1::GFP (a putative orthologue to the mammalian NIX/BNIP3L) which is a key mediator of mitophagy and longevity assurance, and LGG-1::RFP (orthologue to mammalian LC-3) which reports general autophagy. The *atm-1* strain was crossed with N2; *Ex(pmyo-3::dsred::lgg-1;pdct-1::dct-1::gfp)* to generate the *atm-1*; *Ex(pmyo-3::dsred::lgg-1;pdct-1::dct-1::gfp)* strain. The pictures were taken under a fluorescent microscope at 10 X magnification.

(B) Effects of NR (500 μM) on the induction of mitophagy in N2 and *atm-1* worms. N2 and *atm-1* were treated with NR from the L4 stage, followed by confocal imaging on adult D4. A mitochondrial toxicant, paraquat (1 mM, one day treatment), was used as a positive control. Quantification of the data is shown in Figure 4D.

(C) Worms were exposed to *E. coli* with either RNAi control (L4440) or RNAi for two mitophagy genes (*dct-1*, *pink-1*) starting from the egg hatching stage, followed by NR supplementation (500 μM) beginning at the L4 stage. Muscle cells of adult D4 worms of different groups (N2;*ccIs4251* and *atm-1*;*ccIs4251)* were randomly imaged using a confocal microscopy (63X). The *pmyo-3::gfp* of *ccIs4251* expresses at high levels in both the nucleus and mitochondria of body wall muscles. Representative confocal images of muscle mitochondrial network morphology of designated groups are shown.

(D) Arbitrary scoring of mitochondrial network morphology. The value of mitochondrial morphology was given a score from 1~5. The value 1 denotes a severely impaired mitochondrial network, and 5 means a very well-organized mitochondrial network. Results 3.7 ± 0.13 (N2 L4440 veh); 3.98 ± 0.15 (N2 L4440 NR); 2.32 ± 0.15 (*atm-1* L4440 veh); 2.85 ± 0.18 (*atm-1* L4440 NR); 2.74 ± 0.18 (N2 *dct-1* veh); 2.6 ± 0.17 (N2 *dct-1* NR); 2.14 ± 0.16 (*atm-1 dct-1* veh); 2.06 ± 0.16 (*atm-1 dct-1* NR); 2.34 ± 0.16 (N2 *pink-1* veh); 2.16 ± 0.5 (N2 *pink-1* NR); 2.24 ± 0.15 (*atm-1 pink-1* veh); 2.3 ± 0.17 (*atm-1 pink-1* NR); Data shown is mean ± S.E.M. Scoring of the mitochondrial network morphology was conducted blind to the investigator. The experiments were repeated twice with a total of over 50 muscle cells from 20~30 worms imaged.

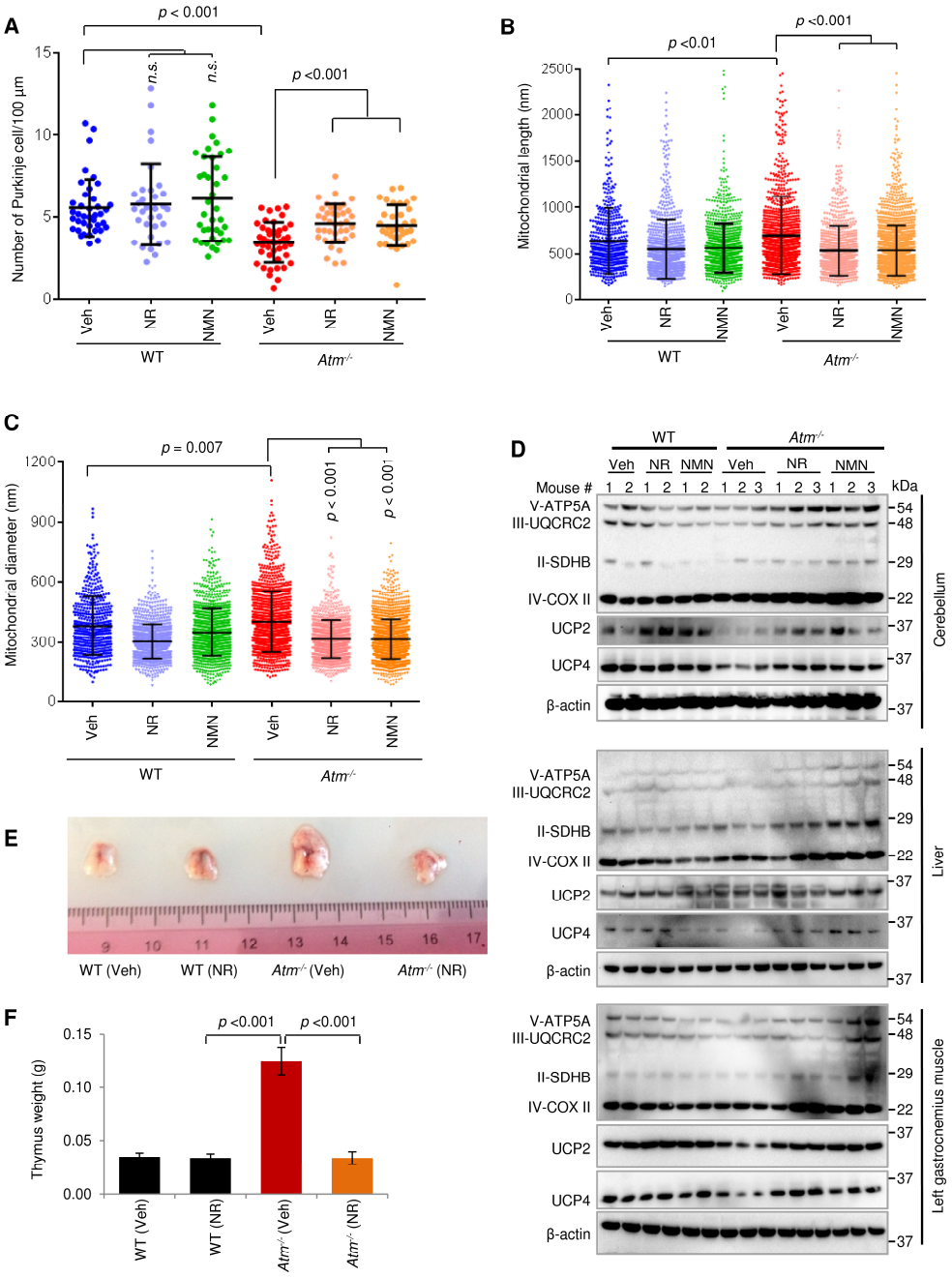

Sup Fig. 5.

Figure S5. Effects of NAD$^+$ augmentation on the phenotypes of *Atm*$^{-/-}$ mice (Related to Figure 7).

WT and *Atm*$^{-/-}$ mice were given NR (12 mM) and NMN (12 mM) in their drinking water starting from weaning and for 14 consecutive days. On D15, mice were euthanized and the tissues were collected for different assays.

(A) Quantification of the numbers of Purkinje cells/100 μm from representative images shown in Fig. 7D. WT veh, 5.56 ± 1.73 (n =39); WT NR, 5.78 ± 2.45 (n=33); WT NMN, 6.09 ± 2.58 (n = 38); ATM^{-} veh, 3.48 ± 1.21 (n = 44); ATM^{-} NR, 4.61 ± 1.16 (n = 40); ATM^{-} NMN, 4.51 ± 1.22 (n = 35); Data shown are mean ± S.D. A total of 3-5 mice/group, 'n' denotes total numbers of random areas analyzed in the group.

(B-C) Quantification of mitochondrial length and diameter from EM images such as those shown in Fig. 7F. Data shown are mean ± S.D. Fourteen pictures for each mouse were taken with 3-5 mice/group, and a total of 559-2000 mitochondria/group were counted. WT veh, n =559; WT NR, n=1000; WT NMN, n = 1245; *Atm*$^{-/-}$, veh, n = 1165; *Atm*$^{-/-}$ NR, n = 960; *Atm*$^{-/-}$ NMN, n = 2000.

(D) Immunoblot analysis of the indicated proteins from the cerebellum, liver, and left gastrocnemius muscle of WT and *Atm*$^{-/-}$ mice on various treatments. Mitochondrial oxidative phosphorylation subunits such as ATP5A, UQCRC2, SDHB and COX2 were evaluated by western blotting. There were increases of the COX2 subunit of complex IV in NR or NMN-treated *Atm*$^{-/-}$ mice in all tissues, while several of the other proteins showed increased expression only in the cerebellum. Since high mitochondrial membrane potential was shown in different ATM-KD cell types, including thymocytes (Valentin-Vega et al., 2012), and neurons (Fig. 1), and membrane potential is in part regulated by the expression of uncoupling proteins, we measured the expression of UCP2 and UCP4. Cerebellum and liver showed increased UCP2 and UCP4 following NR and NMN treatment while liver only showed UCP4 upregulation.

(E-F) The weights of thymus from designated groups. A representative set of thymus tissues are shown in (E), and quantitative data were from 3-5 mice from each group (F).

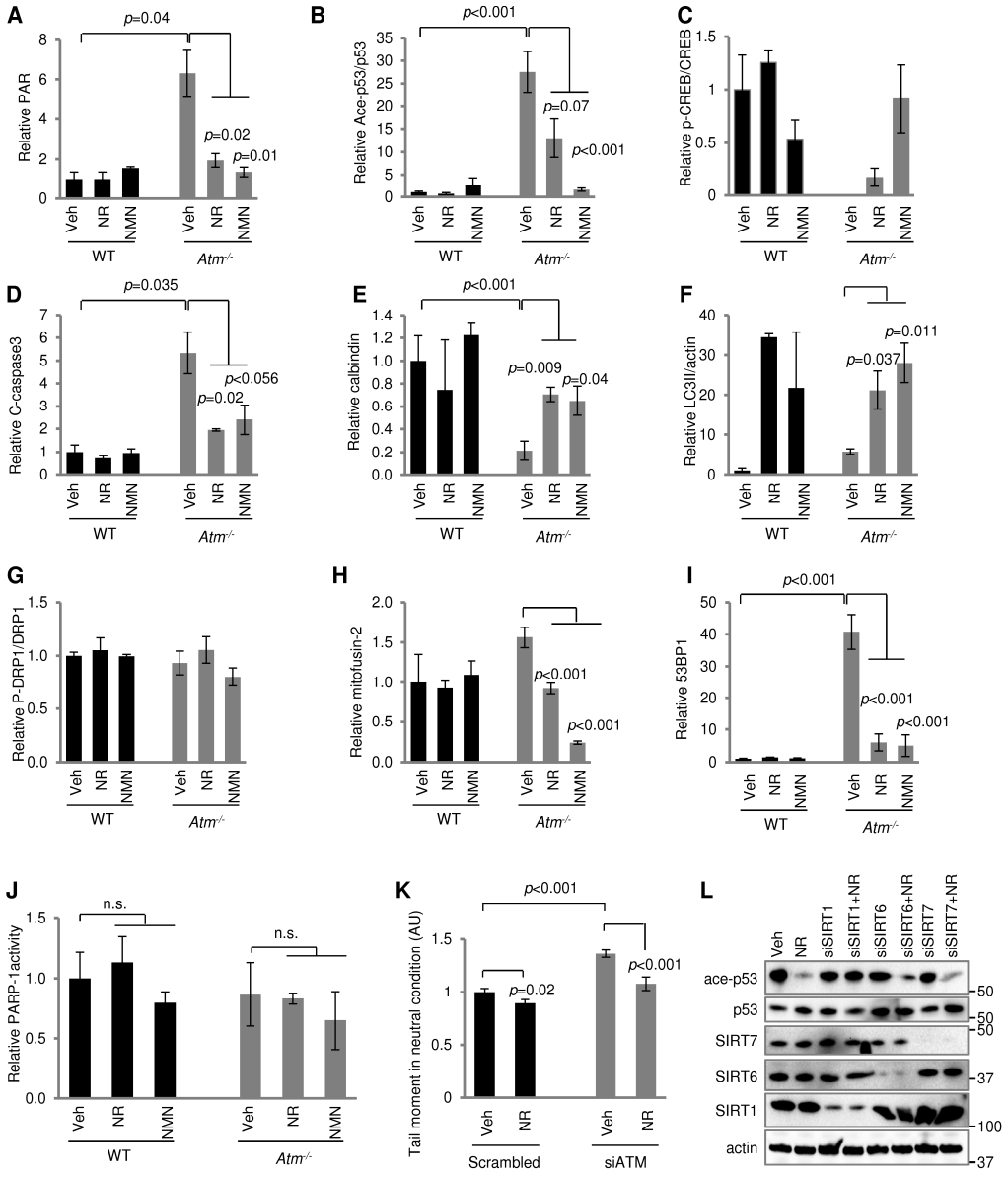

Sup Fig. 6.

Figure S6. Effects of NAD$^+$ precursors on designated antigen levels, relative PARP-1 activity, and steady stage DSBs in *Atm*$^{-/-}$ mice and ATM-KD neurons (Related to Figure 7).

(A-I) Effects of NR and NMN on the expression levels of PAR (A), relative Ace-p53/p53 (B), relative p-CREB/CREB (C), relative Cleaved caspase-3 (D), relative calbindin (E), relative

LC3-II/actin (F), relative p-DRP1/DRP1 (G), relative mitofusin-2 (H), and relative 53BP1 (I) from brain tissues of *Atm*$^{-/-}$ and WT mice. n=3 for each group.

(J) PARP1 activity from brain tissues of *Atm*$^{-/-}$ and WT mice. n=3-5.

(K) Comet assay showing steady state DSBs levels in both WT and ATM-KD neurons with/without NR treatment. Rat cortical neurons at 3 DIV were treated with either scrambled siRNA (siCtrl) or ATM siRNA then treated for 48h with NR at 5 DIV. Neurons were harvested for comet assay on 7 DIV.

(L) Representative western blotting data of indicated proteins in ATM-KD SH-SY5Y cells with designated treatments.

Supplementary Tables

Table S1, related to Figure 3: Commonly changed pathways among NR, SRT and Ola treatments on *atm-1* worms.

There were 70 common pathways changed with all three compounds in *atm-1* worms and 54 of them (77%) were changed in the same direction (A). Within all the 70 common change pathways, 49 of them meet the criterion that at least one condition (NR/SRT/Ola) has a Z-score change ≥ |±1.5| and 90% (44 out of 49) of the pathways changed in the same direction (B).

Table S2, related to Figure 3: Proteins differently expressed in old D10 *atm-1* worms compared to all other conditions (277 proteins, worksheet 1), enriched biological processes of D10 *atm-1* vehicle (worksheet 2), and a list of proteins which fulfilled the 3 criteria ("3C", worksheet 3).

Table S3, related to Figure 3: A list of proteins changed by aging and NR.

Venn diagram analysis of proteomics showing aging has a more profound effect in *atm-1* worms. A comparison between (*atm-1* control day 10 (ACD10) vs. *atm-1* control day 1 (ACD1) and (N2 control day 10 (NCD10) vs. N2 control day 1 (NCD1)) are shown.

Table S4, related to Figure 3: Effects of aging and NAD^+ supplementation on CRH-1 regulated genes in *atm-1* and N2 worms.

CRH-1 regulated genes were previously identified as genes differentially regulated in the *crh-1(nn3315)* null mutant in (PMID: 21331044). Only 7 CRH-1 regulated genes responding to NR treatment in the D1 N2, but a high number of CRH-1 regulated genes are differentially regulated by NR in D10 N2.

Table S5, related to Figure 6: A list of all the metabolites in the mouse cerebellum tissues.

After weaning, *Atm*$^{-/-}$ mice and their WT littermates were exposed to either NR at 12 mM in drinking water or just water. On D15 after compounds exposure, mice were euthanized and the cerebellum tissues were dissected for metabolomics. The metabolome profiles of mouse cerebellum tissues were performed with Capillary electrophoresis/time-of-flight mass spectrometry (CE-TOFMA) and capillary electrophoresis-triple quadrupole mass spectrometry (CE-QqQMS) analysis. Three mice per group were used.

Materials and Methods

Main reagents and antibodies The pEGFP-Pem1-Ad2 reporter plasmid was a gift from Dr. Vera Gorbunova, University of Rochester. The homologous recombination reporter cell line DR-GFP U2OS stable cell line was a gift from Prof. Xiao-fan Wang, Duke University Medical Center. Nicotinamide riboside (Niagen) was from ChromaDex, and nicotinamide mononucleotide was from Sigma and Dr. David Sinclair's laboratory. Olaparib (AZD 2281, #S1060) was from Selleckchem. The siATM, siSIRT1, siSIRT6, siSIRT7 were purchased from Dharmacon or Origene. Worm microarray kits were from Agilent.

Antibodies: BDNF (#sc-546, Santz Cruz); phosphor-CREB (ser133) (#9198, Cell signalling); CREB (#9197, Cell signalling); PSD95 (#ab18258, abcam); Synapsin-1 (#5297p; Cell signalling); actin (#ab6276, Cell signalling or #4967, Cell signalling); ATM (#ab32420, abcam); PAR (#551813, BD Pharmingen^{TM}); PARP-1 (#9542, Cell signalling); SIRT1 (#8469, Cell signalling); Acetylated p53 (Lys379, #2570, Cell signalling); p53 (#sc-71818, Santz Cruz); PGC-1α (#sc-13067; Santz Cruz); acetylated-lysine (Ac-K-103) (#9681, Cell signalling); Sir2.1 (#NB100-1923, Novus); crh-1 (#crh-1, ab-mart); HSP-6 (#hsp-6, ab-mart); acetylated-Ku70 (acetyl K331) (#ab190626, abcam); Ku70 (sc-56129, Santz Cruz); phosphor-DNA-PKcs (ser2056) (#4215, Cell signalling); DNA-PKcs (sc-390849, Santz Cruz); calbindin (ab82815, abcam); anti-Caspase-3 (full length and cleaved; #9662, Cell signalling); cleaved caspase-3 (Asp175) (#9664, Cell signalling); LC3 (#NB 100-2220, Novus); anti-DRP1 (D8H5, #5391, Cell signalling), anti-phospho-DRP1 (ser616, #3455, Cell signalling); anti-mitofusion 2 (#9482, Cell signalling); TUJ-1 (betaIII tubulin) (#ab14545, abcam); 53BP1 (#4937; Cell signalling); COX-4 (#SC-69362, Santz Cruz); UCP2 (#Ab-LS-B3249; Lifespan company); UCP4 (#Ab-LS-C148475; Lifespan company); total OXHOS rodent cocktail (ab110413, abcam); Sirt2 (abcam, #ab51023), Sirt3 (Cell signaling, #5490), Sirt4 (Sigma, #S0948), Sirt5 (Sigma, #HPA022002), Sirt6 (Cell signaling, #12486), Sirt7 (Millipore, #ABE103), Histone H3 (D1H2) (Cell signaling, #4499).

Primary neuronal culture. Primary rat cortical neurons were prepared using a method described elsewhere (Cheng et al., 2016). In brief, cultures of cortical neurons were prepared

from Sprague-Dawley rat embryos at 18 days of gestation. Dissociated cells were seeded into polyethyleneimine-coated plastic dishes or glass coverslips in MEM medium supplemented with 10% fetal bovine serum at a density of 80,000 cells/ cm^2. After cells attached to the substrate, the medium was replaced with Neurobasal medium containing 5% B27, 1% Glutamax and 1% Anti-Anti (Gibco). The neurons were grown in 20% O_2 + 5% CO_2 at 37℃ for further experiments.

Detection of mitochondrial parameters. Rat cortical neurons at 3 days *in vitro* (DIV) were treated with either scrambled siRNA (siCtrl) or ATM siRNA (siATM, Accell siRNA Reagents -rat-E-101032-00-0005) then treated for 48h with designated compounds on 5 DIV, then on 7 DIV the assays for the multiple endpoints were performed. For human SH-SY5Y and U2OS cells, Atm was knockdown using Accell siRNA Reagents-Human#E-003201-00-0005. Different compounds were added to the neurons: Nicotinamide riboside/NR, 500 μM; nicotinamide mononucleotide/NMN, 500 μM; resveratrol/resv, 5 μM; SRT1720/SRT, 2 μM; Olaparib/Ola, 500 nM; or Veliparib/Veli, 500 nM. Cell were incubated with different dyes (all from Life Technologies™), including TMRM (40 nM for 15 min) to detect mitochondrial membrane potential, MitoTracker Green (50 nm for 30 min) for mitochondrial content, dihydroethidium (DHE, 3 μM for 30 min) to detect cellular ROS, and mitoSOX (3 μM for 30 min) for mitochondrial ROS, followed by detection on a plate reader for neurons or by flow cytometer for SY5Y cells (Fang et al., 2014; Hou et al., 2012). For mitochondrial ROS, data were presented as total mitochondrial ROS/cell.

NAD^+ detection. The NAD^+ levels in cells were measured by using a commercial NAD/NADH assay kit (#ab65348) by following the manufacturer's protocol. The NAD Cycling Enzyme Mix in the kit recognizes NADH and NAD, but not NADP or NADPH, in an enzyme cycling reaction. For the mouse cerebellum tissues, NAD^+ levels were quantified by Capillary electrophoresis/time-of-flight mass spectrometry (CE-TOFMA) and capillary electrophoresis-triple quadrupole mass spectrometry (CE-QqQMS) analysis (Human Metabolome Technologies America, Boston).

Immunoblot and immunoprecipitation. Immunoblots were performed per methods previously described (Fang et al., 2014). Briefly, cells were harvested, lysed with RIPA buffer (Cell Signaling) and sonicated. After centrifugation at 14,000 RPM for 30 min at 4 ℃, 50 µg supernatant was denatured at 95 ℃ for 5 min, and then loaded onto an 10-well or 15-well NuPage 4-12 % gel and electrophoresed at 185 V for 1 h, or loaded onto an 18-well or 26-well Bio-rad gel (4–15% Criterion™ TGX™ Gel) and electrophoresed at 150 V for 1h. After SDS-PAGE, gels were transferred at 200 mA for 1~3 h. Membranes were incubated with primary and secondary antibodies. Images were captured using a ChemiDocTM MP system (Bio-Rad) and analyzed with Bio-Rad Image LabTM software. For worm tissues, whole body proteins were extracted using an established method, followed by SDS-PAGE, membrane transfer, and imaging (Arczewska et al., 2013). For the determination of acetylation levels of PGC-1α, immunoprecipitation using an anti-acetyl lysine antibody, followed by immunoblot, detection of PGC-1α with antibody and imaging (Gomes and Sinclair, 2015). Fractionation of subcellular contents from cells was done using a commercial kit (Thermo Fisher Scientific, #78840).

Confocal microscopy. Morphology of neurons, especially neurites, was monitored using a confocal microscope. Neurons were first seeded in 4-well chamber slide (5000~10,000/well) overnight and treated with different reagents for the specified time intervals. Neurons were then washed in cold PBS and fixed with 3.7% paraformaldehyde in PBS for 10 min on ice, and subsequently washed with PBS and permeabilized in 0.25% Triton X-100 for 10 min on ice. Neurons were then blocked in 5% FBS in PBS overnight (4℃) and probed with different primary antibodies (TuJ-1 1:2000 dilution; synapsin 1:1000; 53BP1 1:1000;) at 37℃ for 1 h. Neurons were then washed with PBS x 3 times and probed with fluorescent secondary antibodies (1:1000 dilution) for 1 h at 37℃ before washes with PBS x 6 times. Neurons were mounted in prolong gold anti-fade with DAPI (Invitrogen) and images were taken at 60 × magnification on a Nikon Eclipse TE-2000e confocal microscope (Nikon, Tokyo, Japan). Similarly, neuronal death was measured using cleaved caspase-3

staining (1:500). The Volocity software was used to quantitatively analyze the unbiased global Pearson's coefficients in 15 random images of at least 50 cells.

Electron microscopy for mitochondrial morphology. Electron microscopy was performed by Electron Microscopy Bioservices. For SH-SY5Y cells, they were washed in cold PBS, fixed in EM fixative buffer for 10 min, and subsequently scraped with a cell scraper. Cells were immediately centrifuged into a tight pellet at 2000 RPM for 10 min, and placed at 4 ℃ for an additional 3-h fixation. Fixative buffer was removed and cell pellets were carefully rinsed with Millonig's buffer in triplicate. The cell pellet was then minced post-fixed in 1.0% OsO_4, en bloc stained with 2.0% aqueous uranyl acetate, embedded in Spurr's plastic resin. Ultra-thin section analysis was performed on an electron microscope (Tecnai Spirit Twin Transmission; FEI) at 80 kV. For mouse cerebellum tissues, fresh tissues were fixed with ice-cold 4% formaldehyde solution in PBS overnight, followed by embedding, ultra-thin sectioning, post-staining, and extensive microscopic examination. The percent damaged mitochondria was counted from 14 random images. The mitochondrial length and diameter were measured using ImageJ, n>150. The percent of mitochondria undergoing mitophagy was determined by visualization of engulfed or partially engulfed mitochondria compared with the total mitochondria counted in that sample.

***C. elegans* strains and bacterial strains.** Worms were grown on standard nematode growth medium (NGM) and maintained following standard protocols as described previously (Brenner, 1974). Unless otherwise noted, all experiments utilized *atm-1(gk186)*. The following strains were obtained from the Caenorhabditis Genetics Center (CGC): Bristol N2, VC381 *atm-1(gk186)*I, CB5600 *ccIs4251[pSAK2 (myo-3p::gfp-lacz(NLS)) + psak4 (myo-3p::mitochondrial gfp)*I; *him-8(e1489)* IV, DW102 *brc-1(tm1145)* III, DW103 *brd-1(dw1)* III, FX1524 *cku-70(tm1524)* III, RB964 *cku-80(ok861)* III. The VC199 *sir-2.1(ok434)* IV was a gift from Prof. Johan Auwerx (Ecole Polytechnique Fe´de´rale de Lausanne, Switzerland) (Mouchiroud et al., 2013). The *atm-1*(*gk186);(h2681*) strain was from Prof. Ann Rose

(University of British Columbia, Canada). The mitophagy reporter strain *N2;Ex(pmyo-3::dsred::lgg-1;pdct-1::dct-1::gfp)* was from Prof. N. Tavernarakis (University of Crete, Greece) (Palikaras et al., 2015). The following strains were generated for this study: *atm-1(gk186)*I*;sir-2.1(ok434)*IV, *atm-1(gk186);ccIs4251*I, *atm-1(gk186)*I*;Ex(pmyo-3::dsred::lgg-1;pdct-1::dct-1::gfp).*

RNA interference (RNAI) feeding constructs for L4440 (control), *sir2.1; daf-16; pink-1, pdr-1* and *dct-1* were derived from two RNAi feeding libraries (Dr. Sige Zou's laboratory (previously form NIA) and the other one from Open Biosystems [the *E. coli* host strain is HT115(DE3) (Fire Lab)]). RNAi was performed as previously described with worms maintained on the RNAi from egglaying stage throughout the experiment (Arczewska et al., 2013; Glenn et al., 2004).

Lifespan and healthspan of *C. elegans*. Lifespan examination was performed as described previously (Fang et al., 2014; Fensgard et al., 2010; Kassahun and Nilsen, 2013; Scheibye-Knudsen et al., 2014). Lifespan analysis was performed at 25 ℃ on NGM plates containing 5-fluorodeoxyuridine (5-FdUrd) in the absence or presence of 500 µM NR, 10 µM SRT1720, 500 µM Olaparib, or a combination of 500 µM NR +10 µM SRT1720. Worms were considered dead when they stopped pharyngeal pumping and were unresponsive to touch. The mean, standard deviation of the mean, and P values were calculated using the log-rank test, from pooled population of animals. Figures display Kaplan Meier survival curves of pooled populations utilized for statistical analysis.

Healthspan was performed using two assays, swimming movement and pharyngeal pumping (Bansal et al., 2015; Restif et al., 2014). For swimming movement, worms from a treatment group were randomly selected and transferred to a 6-cm petri dish containing 1 mL of M9 buffer. The worms were allowed to acclimate for ~10 s, then movements were scored for 30 seconds. Pharyngeal pumping was calculated under a microscope (10X) and the numbers of pumps in 30 seconds counted. Rates for pumping and movement were adjusted to counts per minute for analysis. Short-term associative memory (STAM) and long-term associative

memory for the worms were performed as reported previously (Kauffman et al., 2010). To avoid the impact of defective locomotion on the scoring of LTAM/STAM in atm-1 worms, these experiments were performed at an early stage (D1 and D4) when no detectable locomotion defects were observed in atm-1 worms.

***C. elegans* microarray.** For microarray analysis, N2 and *atm-1* worms were exposed to different compounds (vehicle, 500 µM NR, 10 µM SRT1720, 500 nM Olaparib) from L4 stage and after, followed by whole body tissue collection at adult day 1 or adult day 10. Three biological replicates were prepared for each group. The Agilent kits were used for *C. elegans* microarray with the reagents including *C. elegans* (V2) Gene Expression Microarray (# G2519F-020186), Low Input Quick Amp Labeling Kit (one color, #5190-2305), Hybridization Backing Kit (# G2534-60012), and Gene Expression Hybridization Kit (#5188-5242). Total RNA extraction was done using a Qiagen RNeasy mini kit with a QIAcube machine (Kassahun and Nilsen, 2013). The microarray was performed by the Gene Expression and Genomics Unit (NIA) and then analyzed using DIANE 1.0 software (see http://www.grc.nia.nih.gov/branches/rrb/?dna/diane_software.pdf for information). Two samples (Atm1_NR_Day1_3 and N2_SRT1720_Day10_3) were excluded in the analysis since they did not pass the quality analysis. Raw microarray data were log transformed to yield z-scores. The z-ratio was calculated as the difference between the observed gene z-scores for the experimental and the control comparisons, and dividing by the standard deviation associated with the distribution of these differences. Z-ratio values of ± 1.5 were chosen as cut-off values and calculated using a 5% false discovery rate (FDR) threshold. The complete set was tested for gene set enrichment using parametric analysis of gene set enrichment. For each pathway z-score, a p-value was computed using JMP 6.0 software to test for the significance of the z-score obtained.

***C. elegans* proteomics.** Day 1 and 10 N2 and *atm-1* nematodes were cultured in the presence of NR, SRT1720, and Olaparib. Four biological replicates were analyzed. Crude extracts were prepared by bead beating from packed nematode pellets in tissue protein extraction reagent (T-PER, Life Technologies, # 78510) with protease inhibitors. Protein

extracts (25 µg) were precipitated with 400 µl of ice-cold acetone at -20°C. After overnight precipitation, samples were centrifuged at 16,000 g for 30 minutes at 4°C and the supernatant was discarded. Proteins were re-dissolved in 50 µL of 6M urea in 50 mM ammonium bicarbonate, pH 7.8. Subsequently, 2.5 µL of 200 mM DTT (Sigma-Aldrich, Oslo, Norway) was added and the samples were incubated for 30 min at 30°C to reduce the disulfide bridges. Thiols were then alkylated with 7.5 µL of 200 mM iodoacetamide (IAA Sigma-Aldrich, Oslo, Norway) (1h, 30°C, dark), following which the excess of IAA was quenched with 10 µL of 200 mM DTT (30 min, 30°C). After reducing the urea concentration down to 1M, proteins were digested with sequencing grade modified trypsin (Promega, Madison, WI, USA) for 1 h at 37°C, followed by 15 h incubation at 30°C. The digestion was terminated by adding 5 µL of 50 % formic acid and the generated peptides were purified using a Strata C18-E SPE column (Phenomenex, Værløse, Denmark), and dried using a Speed Vac concentrator (Eppendorf, Hamburg, Germany).

Liquid chromatography-mass spectrometry (LC-MS)

Tryptic digests from four replicates of each sample were analyzed using an Ultimate 3000 nano-UHPLC system (Dionex, Sunnyvale, CA, USA) connected to a Q Exactive mass spectrometer (ThermoElectron, Bremen, Germany) equipped with a nano electrospray ion source. For liquid chromatography separation, an Acclaim PepMap 100 column (C18, 3 µm beads, 100 Å pore size, 75 µm inner diameter, 50 cm length) was used. A flow rate of 300 nL/min was employed with a solvent gradient of 4-35% B in 207 min, to 50% B in 20 min and then to 80% B in 2 min. Solvent A was aqueous 0.1% formic acid and solvent B contained 0.1% formic acid in 90% acetonitrile. The mass spectrometer was operated in the data-dependent mode to automatically switch between MS and MS/MS acquisition. Survey full scan MS spectra (from m/z 300 to 2000) were acquired in the Orbitrap with resolution R = 70,000 at m/z 200, after accumulation to a target of 1,000,000 ions in the C-trap. The maximum allowed ion accumulation times were 100 ms. The method used allowed sequential isolation of up to the ten most intense ions, depending on signal intensity (intensity threshold $1.7e^4$), for fragmentation using higher collision induced dissociation (HCD) at a target value of $1e^5$ charges and a resolution R = 17,500. Target ions already selected for MS/MS were dynamically excluded for 60 sec. The isolation window was 2 *m/z* units without

offset. The maximum allowed ion accumulation for the MS/MS spectrum was 60 ms. For accurate mass measurements, the lock mass option was enabled in MS mode and the polydimethylcyclosiloxane ions generated in the electrospray process from ambient air were used for internal recalibration during the analysis.

Data analysis for *C. elegans* proteomics

Data were acquired using Xcalibur v2.5.5 and raw files were processed to generate peak list in Mascot generic format (.mgf) using ProteoWizard release version 3.0.331. Database searches were performed using Mascot in-house version 2.4.0 to search the SwissProt database (Caenorhabditis elegans, 19.05.2015, 26156 proteins) assuming the digestion enzyme trypsin, at maximum one missed cleavage site, fragment ion mass tolerance of 0.02 Da, parent ion tolerance of 10 ppm and oxidation of methionine, acetylation of the protein N-terminus as variable modifications and carbamidomethylation of cysteine as fixed modification. Scaffold (version Scaffold_4.3.4, Proteome Software Inc., Portland, OR) was used to validate MS/MS based peptide and protein identifications. Peptide identifications were accepted if they could be established at greater than 95.0% probability by the Scaffold Local FDR algorithm. Protein identifications were accepted if they could be established at greater than 99.0% probability. The mass spectrometry proteomics data have been deposited to the ProteomeXchange Consortium via the PRIDE partner repository with the dataset identifier PXD003380.

Fecundity and male frequency. For brood size and male frequency assays, animals were transferred daily to fresh new plates supplemented with agents (500 µM NR, 10 µM SRT1720, 500 nM Olaparib) or vehicle control during the reproductive period and progeny and male numbers were counted. Data present the average of at least 3 independent trails.

NHEJ in *C. elegans*. This is an adaptation of the somatic cell NHEJ repair assay (Clejan et al., 2006) in which embryonic NHEJ capacity is measured by scoring the slow growth (Gro) phenotype 48 h post irradiation. Briefly, L4 larvae were picked and allowed to mature to fecund adults in the presence of 500 µM NR, 10 µM SIRT1720 and 500 nM Olaparib. 10

well-fed young adults were transferred to a new plate supplemented with the drugs and allowed to lay eggs for 2 h. Subsequently, adults were removed from the plate and eggs were allowed to develop for 3 h to become late-stage embryos prior to irradiation with 90 Gy. Gamma irradiation was performed in a Gammacell 40 Exactor irradiator at a dose rate of 79.37 rads/min. Numbers of eggs that hatched and grew into L4 stage were counted, with growth rate indicated as percent of eggs grew into L4 stage/total eggs.

Detection of mitophagy in cells and *C. elegans*. Several methods were used to detect mitophagy in primary neurons, SH-SY5Y cells and *C. elegans*. Electron microscopy was used to calculate the percent of mitochondria undergoing mitophagy by visualization of engulfed or partially engulfed mitochondria compared with the total mitochondria counted in that sample (method described above). Alternatively, colocalization of the autophagy marker LC3 and a mitochondrial marker COX-4 was also used quantify mitophagy (Fang et al., 2014). In worms, the mitophagy reporter strain *N2;Ex(pmyo-3::dsred::lgg-1;pdct-1::dct-1::gfp)* was crossed with *atm-1(gk186)*. Worms were exposed to different compounds at L4 stage, followed by imaging of muscle cells at day 4. Worms were treated 24 h with 1 mM Paraquat (PQ) as a positive control (Palikaras et al., 2015). A total of 15~20 worms/group were imaged in two independent replicates. Colocalization coefficient between DSRED::DCT1 and LGG1::GFP were analyzed using the Zeiss LSM Image Examiner. Imaging of mt-mKeima cells (gift from Dr. Richard Youle) was performed as reported by Nuo and colleagues (Sun et al., 2015), using different settings for GFP (alkaline condition, excitation 458 nm and emission 615 nm) and RFP (acidic condition, excitation 561 nm and emission 615 nm).

Mitochondrial network morphology in *C. elegans*. A *myo-3::gfp* reporter strain was used for mitochondrial networking morphology analysis in the body wall muscle cells. Worms were treated with the designated drugs from L4 stage for 4 days followed by imaging with a Zeiss confocal microscopy. We imaged over 15 worms/group each time, and it was repeated twice. Arbitrary score for mitochondrial network was performed in a double-blinded manner. A score from 1 to 5 was set. A score of 5 denotes a perfectly organized mitochondrial

network with healthy mitochondria running parallel with the myofilament lattice. For highly fragmented and disorganized mitochondrial network morphology, a score of 1 was given.

DNA damage and repair in cells. Quantification of DNA double-strand breaks (DSBs) in neurons was performed using neutral comet assays (Sykora et al., 2015). For the *in vivo* NHEJ assay, rat primary neurons were seeded (1 x 10^5 cells) and transfected with 200 ng of pEGFP-Pem1-Ad2 reporter plasmid (gift from Dr. V. Gorbunova, University of Rochester) digested with HindIII or I-SceI (New England Biologicals) and 25 ng of pDSRed-Express-C1 (Clonetech) using Lipofectamine 3000 (Lifetechnologies) and OptiMEM (Seluanov et al., 2004). Four hours post-transfection, cells were supplemented with fresh media. GFP positive and DsRed positive cells were counted using microscope after three days of transfection and NHEJ efficiency was calculated by normalizing GFP positive cells to DsRed positive cells (Dobbin et al., 2013).

***Atm* mice maintenance.** The Atm heterozygous strain (B6;129S4-*Atm*^{tm1Bal}/J , #stock number 020943) was purchased from The Jacksons Laboratory. We bred the Atm heterozygous to generate Atm homozygous (*Atm*$^{-/-}$) mice and their wild type (WT) littermates, both were used for experiments. For genotyping, primers for WT included primer #16338 (GGT CTC CAG CCT TAA CCA CA) and primer #16339 (TCC TGC TGA TGT GTC TGA CC) which produce a product of 473 bp; for mutant allele the primers were #16339 (TCC TGC TGA TGT GTC TGA CC) and #OLMR2088 (AGA CTG CCT TGG GAA AAG CG) which generates a product of around 600 bp (http://jaxmice.jax.org/strain/020943.html). All the animals were maintained at the National Institute on Aging under standard conditions and fed standard animal chow. All animal experiments were performed and approved by NIA Animal Care and Use Committee.

Lifespan and behavioral studies of *Atm*$^{-/-}$ mice. The *Atm*$^{-/-}$ male mice and their age- and sex-matched littermates were used for both lifespan and behavioral studies. For lifespan

studies, after weaning the mice were given nicotinamide riboside (NR) at 3.5 mg/ml (12 mM) in their drinking water while the control groups were received only drinking water. The NR water solution was filtered and the bottles were covered with foil. Fresh NR solution was replaced every 2~3 days. Mice were monitored every day and weighted every two weeks. Dead mice were recorded, and necropsied. Lifespan curves were generated using Kaplan Meier method.

For healthspan studies, after weaning the mice were given nicotinamide riboside (NR) at 3.5 mg/ml (12 mM) or 4.02 mg/ml (12 mM) nicotinamide mononucleotide in their drinking water while the control groups were received only drinking water for 14 days. On day 14 the behavioral studies were completed, these included rotarod testing for motor performance and the Y maze assay for Spontaneous Alternation Performance test (SAP) (Ghosal et al., 2009). For the rotarod test, day 14 treated or vehicle control mice were placed onto the ENV-577M Rotarod system (Med Associates, Georgia) at a walking speed of 4 rpm then the system increased the speed to 40 rpm in 300 seconds. The time spent on the rotarod was recorded (Cheng et al., 2016). The Y Maze SAP is a behavioral test that measures the willingness of mice to explore a new environment. Mice were introduced to the center of the Y maze to allow them to freely explore the three arms, labelled A, B, and C. For each mouse, the test was carried out for 5 min, and the testing surface was cleaned with 75% ethanol between each trial. SAP is the subsequent entry into a novel arm over the course of 3 entries and the % SAPs is calculated by the number of actual alternations/(total arm entries-2) X 100 (Ghosal et al., 2009; Gotz and Ittner, 2008).

Histology and electron microscopy on mouse brain tissues. The $Atm^{-/-}$ and WT mice were anesthetized, dissected, and fixed with 4% cold paraformaldehyde in PBS (pH 7.4) for 24 h. Tissues were then transferred to a cryopreservation solution (30% sucrose in PBS) at 4 ℃ for 2~5 days until the brains sank to the bottom. The tissues were then transferred to a 1:1 mixture of OCT: sucrose for 1-2 hours. Tissue was then embedded in the mold with OCT, and 16 μm sagittal cryosections were mounted on Superfrost Plus slides (Digger). For staining, brain slices were successively fixed in 95% alcohol, 75% alcohol and 50% alcohol

for 5-7 quick dips at each step then the tissue was stained with 0.5% cresyl violet (Sigma, C5042) solution for 2–5 min. Brain slices were successively dehydrated in 50% alcohol , 70% alcohol, 95% alcohol, for 5-7 quick dips at each step and finally in 100% alcohol for 1 min. Slices were cleared in xylene for 5 min before being covered with coverslip. The number of Purkinje cells per 100 □m was determined for each sample (Louis et al., 2013; Tsai et al., 2012). Typically 10 images were evaluated per sample and 3-5 mice per group. For electron microscopy (EM) of mitochondrial morphology of the brain cerebellum tissues, the tissues were freshly dissected and fixed in 2% paraformaldehyde, followed by EM as aforementioned.

Metabolomics. Metabolomics using both whole worm tissues and mouse cerebellum tissues were performed. To evaluate changes of metabolome in ATM deficiency, whole body tissues of adult Day 6 N2 and atm-1 worms with/without nicotinamide mononucleotide (NMN)/NR treatment (500 μM for L4 stage), were performed at UC Davis Genome Center Core Facilities using ALEX-CIS GCTOF mass spectrometry. Data were then normalized by providing first a variant of a 'vector normalization' in which we calculated the sum of all peak heights for all identified metabolites (but not the unknowns) for each sample. We called such peak-sums "mTIC" in analogy to the term TIC used in mass spectrometry (for 'total ion chromatogram'), but with the notification "mTIC" to indicate that we only used genuine metabolites (identified compounds) in order to avoid using potential non-biological artifacts for the biological normalizations, such as column bleed, plasticizers or other contaminants. Subsequently, we determined if the mTIC averages are significantly different between treatment groups or cohorts. If these averages indeed are different by $p<0.05$, data will be normalized to the average mTIC of each group. If averages between treatment groups or cohorts are not different, or if treatment relations to groups are kept blinded, data will be normalized to the total average mTIC. The semi-quantified metabolome data were finally normalized to the expression of a mitochondrial protein.

The mice were treated with NR (12 mM) in drinking water for 14 consecutive days then sacrificed on day 15. Control mice received only sterilized drinking water. Mouse cerebellum tissues were then extracted and flash frozen and sent to Human Metabolome Technologies

Inc. (Boston) for analysis. Metabolomics for mouse cerebellum tissues was performed using a CE-TOFMS and CE-QqQMS analysis. Data were analyzed as reported elsewhere (Kim et al., 2015; Takebe et al., 2013). Three mice were used per group.

PARP1 activity. PARP-1 was purified from the brain tissues of *Atm*$^{-/-}$ and WT mice through immunoprecipitation, followed by detection of its maximal activity using the Universal Chemiluminescent PARP Assay Kit (Trevigen, #4676-096-K). Signals were monitored using an EnSpire 2300 Multilabel reader (Perkin Elmer).

Statistical Analysis

Statistical analysis used in this study was two-tailed unpaired t-test for comparison between two groups, or ANOVA for comparison among multiple groups. All data were presented as mean ± S.D. **or** mean ± S.E.M. as indicated with p value < 0.05 was considered statistically significant. For lifespan studies, p values were derived from log-rank calculations.

Additional References

Arczewska, K.D., Tomazella, G.G., Lindvall, J.M., Kassahun, H., Maglioni, S., Torgovnick, A., Henriksson, J., Matilainen, O., Marquis, B.J., Nelson, B.C*., et al.* (2013). Active transcriptomic and proteomic reprogramming in the C. elegans nucleotide excision repair mutant xpa-1. Nucleic acids research *41*, 5368-5381.

Bansal, A., Zhu, L.J., Yen, K., and Tissenbaum, H.A. (2015). Uncoupling lifespan and healthspan in Caenorhabditis elegans longevity mutants. Proceedings of the National Academy of Sciences of the United States of America *112*, E277-286.

Brenner, S. (1974). The genetics of Caenorhabditis elegans. Genetics *77*, 71-94.

Cheng, A., Yang, Y., Zhou, Y., Maharana, C., Lu, D., Peng, W., Liu, Y., Wan, R., Marosi, K., Misiak, M*., et al.* (2016). Mitochondrial SIRT3 Mediates Adaptive Responses of Neurons to Exercise and Metabolic and Excitatory Challenges. Cell metabolism *23*, 128-142.

Clejan, I., Boerckel, J., and Ahmed, S. (2006). Developmental modulation of nonhomologous end joining in Caenorhabditis elegans. Genetics *173*, 1301-1317.

Dobbin, M.M., Madabhushi, R., Pan, L., Chen, Y., Kim, D., Gao, J., Ahanonu, B., Pao, P.C., Qiu, Y., Zhao, Y*., et al.* (2013). SIRT1 collaborates with ATM and HDAC1 to maintain genomic stability in neurons. Nature neuroscience *16*, 1008-1015.

Fang, E.F., Scheibye-Knudsen, M., Brace, L.E., Kassahun, H., SenGupta, T., Nilsen, H., Mitchell, J.R., Croteau, D.L., and Bohr, V.A. (2014). Defective mitophagy in XPA via PARP-1 hyperactivation and NAD(+)/SIRT1 reduction. Cell *157*, 882-896.

Fensgard, O., Kassahun, H., Bombik, I., Rognes, T., Lindvall, J.M., and Nilsen, H. (2010). A two-tiered compensatory response to loss of DNA repair modulates aging and stress response pathways. Aging *2*, 133-159.

Ghosal, K., Vogt, D.L., Liang, M., Shen, Y., Lamb, B.T., and Pimplikar, S.W. (2009). Alzheimer's disease-like pathological features in transgenic mice expressing the APP intracellular domain. Proceedings of the National Academy of Sciences of the United States of America *106*, 18367-18372.

Glenn, C.F., Chow, D.K., David, L., Cooke, C.A., Gami, M.S., Iser, W.B., Hanselman, K.B., Goldberg, I.G., and Wolkow, C.A. (2004). Behavioral deficits during early stages of aging in Caenorhabditis elegans result from locomotory deficits possibly linked to muscle frailty. The journals of gerontology Series A, Biological sciences and medical sciences *59*, 1251-1260.

Gomes, A.P., and Sinclair, D.A. (2015). Measuring PGC-1alpha and its acetylation status in mouse primary myotubes. Methods in molecular biology *1241*, 49-57.

Gotz, J., and Ittner, L.M. (2008). Animal models of Alzheimer's disease and frontotemporal dementia. Nature reviews Neuroscience *9*, 532-544.

Hou, Y., Ouyang, X., Wan, R., Cheng, H., Mattson, M.P., and Cheng, A. (2012). Mitochondrial superoxide production negatively regulates neural progenitor proliferation and cerebral cortical development. Stem cells *30*, 2535-2547.

Kassahun, H., and Nilsen, H. (2013). Active transcriptomic and proteomic reprogramming in the C. elegans nucleotide excision repair mutant xpa-1. Worm *2*, e27337.

Kauffman, A.L., Ashraf, J.M., Corces-Zimmerman, M.R., Landis, J.N., and Murphy, C.T. (2010). Insulin signaling and dietary restriction differentially influence the decline of learning and memory with age. PLoS biology *8*, e1000372.

Kim, D., Fiske, B.P., Birsoy, K., Freinkman, E., Kami, K., Possemato, R.L., Chudnovsky, Y., Pacold, M.E., Chen, W.W., Cantor, J.R*., et al.* (2015). SHMT2 drives glioma cell survival in ischaemia but imposes a dependence on glycine clearance. Nature *520*, 363-367.

Louis, E.D., Babij, R., Lee, M., Cortes, E., and Vonsattel, J.P. (2013). Quantification of cerebellar hemispheric purkinje cell linear density: 32 ET cases versus 16 controls. Movement disorders : official journal of the Movement Disorder Society *28*, 1854-1859.
Mouchiroud, L., Houtkooper, R.H., Moullan, N., Katsyuba, E., Ryu, D., Canto, C., Mottis, A., Jo, Y.S., Viswanathan, M., Schoonjans, K*., et al.* (2013). The NAD(+)/Sirtuin Pathway Modulates Longevity through Activation of Mitochondrial UPR and FOXO Signaling. Cell *154*, 430-441.
Palikaras, K., Lionaki, E., and Tavernarakis, N. (2015). Coordination of mitophagy and mitochondrial biogenesis during ageing in C. elegans. Nature *521*, 525-528.
Restif, C., Ibanez-Ventoso, C., Vora, M.M., Guo, S., Metaxas, D., and Driscoll, M. (2014). CeleST: computer vision software for quantitative analysis of C. elegans swim behavior reveals novel features of locomotion. PLoS computational biology *10*, e1003702.
Scheibye-Knudsen, M., Mitchell, S.J., Fang, E.F., Iyama, T., Ward, T., Wang, J., Dunn, C.A., Singh, N., Veith, S., Hasan-Olive, M.M*., et al.* (2014). A High-Fat Diet and NAD(+) Activate Sirt1 to Rescue Premature Aging in Cockayne Syndrome. Cell metabolism *20*, 840-855.
Seluanov, A., Mittelman, D., Pereira-Smith, O.M., Wilson, J.H., and Gorbunova, V. (2004). DNA end joining becomes less efficient and more error-prone during cellular senescence. Proceedings of the National Academy of Sciences of the United States of America *101*, 7624-7629.
Sun, N., Yun, J., Liu, J., Malide, D., Liu, C., Rovira, II, Holmstrom, K.M., Fergusson, M.M., Yoo, Y.H., Combs, C.A*., et al.* (2015). Measuring In Vivo Mitophagy. Molecular cell *60*, 685-696.
Sykora, P., Misiak, M., Wang, Y., Ghosh, S., Leandro, G.S., Liu, D., Tian, J., Baptiste, B.A., Cong, W.N., Brenerman, B.M*., et al.* (2015). DNA polymerase beta deficiency leads to neurodegeneration and exacerbates Alzheimer disease phenotypes. Nucleic acids research *43*, 943-959.
Takebe, T., Sekine, K., Enomura, M., Koike, H., Kimura, M., Ogaeri, T., Zhang, R.R., Ueno, Y., Zheng, Y.W., Koike, N*., et al.* (2013). Vascularized and functional human liver from an iPSC-derived organ bud transplant. Nature *499*, 481-484.
Tsai, P.T., Hull, C., Chu, Y., Greene-Colozzi, E., Sadowski, A.R., Leech, J.M., Steinberg, J., Crawley, J.N., Regehr, W.G., and Sahin, M. (2012). Autistic-like behaviour and cerebellar dysfunction in Purkinje cell Tsc1 mutant mice. Nature *488*, 647-651.
Valentin-Vega, Y.A., Maclean, K.H., Tait-Mulder, J., Milasta, S., Steeves, M., Dorsey, F.C., Cleveland, J.L., Green, D.R., and Kastan, M.B. (2012). Mitochondrial dysfunction in ataxia-telangiectasia. Blood *119*, 1490-1500.